Molecular Neurobiology (2019) 56:102–118
https://doi.org/10.1007/s12035-018-1072-2

Slow Release of HIV-1 Protein Nef from Vesicle-like Structures Is Inhibited by Cytosolic Calcium Elevation in Single Human Microglia

Matjaž Stenovec[1,2] · Eva Lasič[2] · Pia Pužar Dominkuš[3] · Saša Trkov Bobnar[1,2] · Robert Zorec[1,2] · Metka Lenassi[3] · Marko Kreft[1,2,4]

Received: 6 February 2018 / Accepted: 9 April 2018 / Published online: 21 April 2018

Abstract

Once infected by HIV-1, microglia abundantly produce accessory protein Nef that enhances virus production and infectivity, but little is known about its intracellular compartmentalization, trafficking mode(s), and release from microglia. Here, we transfected immortalized human microglia with a plasmid encoding Nef tagged with green fluorescent protein (Nef.GFP) to biochemically and microscopically identify Nef.GFP-associated cellular compartments and examine their mobility and Nef release from cultured cells. Immunoblotting revealed that Nef.GFP confined to subcellular fractions with a buoyant density similar to organelles positive for lysosomal-associated membrane protein 1 (LAMP1) but structurally segregated from dextran-laden and LysoTracker-laden endo-/lysosomes in live cells. As revealed by confocal microscopy, Nef.GFP-positive vesicle-like structures were smaller than dextran-laden vesicles and displayed slow and non-directional mobility, in contrast to the faster and directional mobility of dextran-laden vesicles. Ionomycin-evoked elevation in intracellular free Ca^{2+} concentration ($[Ca^{2+}]_i$) negligibly affected mobility of Nef.GFP structures but strongly and irrecoverably attenuated mobility of dextran-laden vesicles. A slow time-dependent decrease in the number of Nef.GFP-positive structures was observed in non-stimulated controls (5 ± 1 structures/min), but not in ionomycin-stimulated cells (0 ± 2 structures/min; $P < 0.05$), indicating that elevated $[Ca^{2+}]_i$ inhibits the release of Nef.GFP structures. The latter significantly co-localized with membrane sites immunopositive for the tetraspanins CD9 ($36 \pm 4\%$) and CD81 ($22 \pm 1\%$). This is the first report to demonstrate that microglial CD9- and CD81-positive plasma membrane-derived compartments are associated with biogenesis and Nef release.

Keywords Nef · Extracellular vesicles · Microglia · Vesicle mobility · Secretion · Cytosolic calcium activity

Electronic supplementary material The online version of this article (https://doi.org/10.1007/s12035-018-1072-2) contains supplementary material, which is available to authorized users.

✉ Robert Zorec
robert.zorec@mf.uni–lj.si

✉ ?Metka Lenassi
metka.lenassi@mf.uni–lj.si

✉ Marko Kreft
marko.kreft@mf.uni–lj.si

Matjaž Stenovec
matjaz.stenovec@mf.uni-lj.si

Eva Lasič
eva.lasic@mf.uni-lj.si

Pia Pužar Dominkuš
pia.puzar-dominkus@mf.uni-lj.si

Saša Trkov Bobnar
sasa.trkov@mf.uni-lj.si

[1] Celica Biomedical, Tehnološki park 24, 1000 Ljubljana, Slovenia

[2] Laboratory of Neuroendocrinology-Molecular Cell Physiology, Institute of Pathophysiology, Faculty of Medicine, University of Ljubljana, Zaloška 4, 1000 Ljubljana, Slovenia

[3] Institute of Biochemistry, Faculty of Medicine, University of Ljubljana, Vrazov trg 2, 1000 Ljubljana, Slovenia

[4] CPAE, Department of Biology, Biotechnical Faculty, University of Ljubljana, Večna pot 111, 1000 Ljubljana, Slovenia

Introduction

HIV-1 infection of the central nervous system is associated with a spectrum of pathologies, collectively termed HIV-associated neurological disorders (HAND), which lead to attention deficit, behavioral changes, and memory impairments [1]. Microglia, macrophage-like brain-resident immune cells, are pivotal in HAND, as they are the major target for HIV-1 infection [2] and produce inflammatory mediators believed to be the primary cause of neuronal injury or dysfunction [3]. The HIV-1 accessory protein Nef (27–34 kDa) is the first viral protein detectable after HIV-1 infection [4] that not only enhances virus production and infectivity but also exerts effects unrelated to viral replication [5, 6].

For all its known functions, Nef must be first recruited to membranes via amino-terminal myristoylation that occurs co-translationally and is believed to be a "permanent" protein modification. Nevertheless, a large proportion of lipidated Nef (60–75%) seems to remain cytosolic in Nef-expressing cells [7, 8]. When associated with membranes, Nef exposes a relatively large surface area for protein-protein interactions [9] and binds to a multitude of host proteins, including plasma membrane receptors, sorting receptors, and signaling proteins [10]. Nef may further access several intracellular organelles including endosomes, lysosomes [11, 12], and multivesicular bodies (MVBs) [13, 14] that may subsequently fuse with lysosomes. Alternatively, MVBs fuse with the plasma membrane and release their intraluminal vesicles termed exosomes [15].

In vitro, Nef stimulates its own export via the release of extracellular vesicles (EVs) by yet unknown cellular mechanism from Nef-expressing and/or HIV-1-infected T cells [16, 17], peripheral blood mononuclear cells [18, 19], astrocytes [20], and a recent study also suggested release from microglia [21]. Elevated and non-declining levels of plasma EVs containing the viral proteins Nef and Vpu also sustain EV release from HIV-infected cells in vivo. Once released from cells, Nef-positive EVs may trigger apoptosis in bystander T cells [16, 17], contribute to virus infectivity [22], inflammation [18], neurotoxicity [23–25], and impair the blood-brain barrier [21].

In brain microglia, the association of Nef with intracellular membranes and its trafficking mode(s) preceding release are largely unknown. We thus transfected immortalized cultured human microglia (h-microglia), which display numerous characteristics similar to primary microglia [26], with a plasmid encoding Nef tagged with green fluorescent protein (Nef.GFP). Transfected cells expressing Nef.GFP were studied either by cell fractionation and immunoblot assays or by confocal microscopy to examine the subcellular localization, mobility, and release of Nef.GFP. Although murine primary microglia can be used to study certain brain pathologies, HIV-1 displays a remarkably narrow tropism in terms of species and tissues that can be productively infected, necessitating the use of cells of human origin [27, 28]. As revealed by immunoblot assays, Nef.GFP in h-microglia was predominantly localized to subcellular fractions with a similar buoyant density as organelles immunopositive for lysosomal-associated membrane protein 1 (LAMP1), but structurally segregated from dextran-laden and LysoTracker-labelled endo-/lysosomes, as revealed by confocal microscopy. In live cells, Nef.GFP was localized to numerous vesicle-like structures that were smaller in diameter than dextran-laden endosomes and predominantly localized in close proximity to the FM4-64-stained plasma membrane. Nef.GFP structures displayed slow and non-directional mobility, in contrast to the fast and directional mobility of dextran-laden vesicles monitored in the same cells. Ionomycin-evoked elevations in $[Ca^{2+}]_i$ negligibly affected mobility of Nef.GFP structures, but strongly and irrecoverably attenuated mobility of dextran-laden vesicles. Finally, ionomycin stimulation inhibited the time-dependent decrease in the number of Nef.GFP structures in the cells, indicating slow and discrete release of Nef-positive particles (EVs) from h-microglia.

Materials and Methods

Cell Culture

Immortalized (SV40/hTERT) h-microglia, isolated from fresh human cerebral cortex tissue, were developed [26] and kindly provided by the Jonathan Karn laboratory (Western Reserve University, Cleveland, USA). For fractionation and immunoblot analysis, cells were cultivated at 37 °C and 5% CO_2/95% air in Dulbecco's modified Eagle's medium (DMEM, Sigma-Aldrich, St. Louis, MO, USA), supplemented with 1× Glutamax (Thermo Fisher Scientific, Waltham, MA, USA), 10% heat-inactivated and sterile-filtered fetal bovine serum (FBS, Sigma-Aldrich), 100 U/mL penicillin, and 100 μg/mL streptomycin (Amersco, Solon, OH, USA). For EV isolation experiments, EV-depleted FBS was prepared by overnight ultracentrifugation at 100,000×*g* (4 °C) and additionally filtered through 0.22-μm filters (Corning, New York, USA). For imaging experiments, cells were grown in high-glucose DMEM containing 10% FBS (Biochrom AG, Berlin, Germany), 1 mM sodium pyruvate, 2 mM L-glutamine, and 5 U/mL penicillin/5 μg/mL streptomycin in an atmosphere of 5% CO_2/95% air and subcultured every 7 days. Before experimentation, cells were trypsinized, plated onto poly-L-lysine-coated coverslips, and maintained at 37 °C in an atmosphere of 5% CO_2/95% air.

Subcellular Fractionation and Extracellular Vesicle Isolation

For Nef.GFP protein expression, h-microglia were grown overnight to approximately 80% confluence, after which they

were trypsinized (Trypsin-EDTA, Thermo Fisher Scientific), washed with DPBS, and re-suspended in supplemented DMEM to 0.5×10^6 cells per mL. Per each reaction, 2.5×10^6 cells were transfected with 10 μg of the plasmid encoding green fluorescent protein (GFP; pGFP) or the plasmid encoding wild type Nef tagged with GFP (pNef.GFP; [16]) in 25 μL of jetPRIME transfection reagent (Polyplus-transfection, Illkirch, France) mixed with 575 μL of reaction buffer, according to the manufacturer's instructions, and plated. After 4 h, attached cells were washed with DPBS, vesicle-free DMEM with supplements was added, and cells were incubated for another 48 h at 37 °C.

For subcellular fractionation, cells were trypsinized, centrifuged at 800×*g* for 5 min, and washed with DPBS and fractionation buffer (0.25 M sucrose, 1 mM EDTA, 10 mM Tris-HCl, pH 7.4). Next, cells were re-suspended in 1 mL of cold fractionation buffer supplemented with protease inhibitors (PIs, Sigma-Aldrich) and homogenized using a Dounce homogenizer (30 strokes, 4 °C). Homogenate was centrifuged at 1000×*g* for 5 min at 4 °C to pellet nuclei and larger cellular fragments (nuclear fraction; Nuc) at 15,000×*g* for 15 min to pellet mitochondria, lysosomes, peroxisomes, Golgi membranes, endoplasmic reticulum, and endosomes (light mitochondrial fraction; LMF), and at 100,000×*g* for 70 min (TLA-55, BC) to pellet cytoplasmic vesicles and microsomes (vesicle fraction; Ves). The remaining supernatant contained cytosolic proteins (cytosolic fraction; Cyt), which were precipitated using trichloroacetic acid and sodium deoxycholate (TCA/DOC). Alternatively, the LMF fraction was re-suspended in a total volume of 700 μL DPBS supplemented with PI, transferred on top of the 15–25% iodixanol density gradient (Optiprep, Sigma-Aldrich), and ultracentrifuged at 100,000×*g* for 19 h at 4 °C (MLS-50, Beckman Coulter, BC). Seventeen 290 μL fractions were collected from the top of the gradient and proteins confined to particular fractions precipitated with TCA/DOC.

For EV isolation, the culture medium was collected after the 48 h incubation and centrifuged at 800×*g* for 5 min to remove cells and at 2500×*g* for 15 min to remove apoptotic bodies. EVs were next pelleted by ultracentrifugation at 100,000×*g* for 1 h at 4 °C (MLA-50, BC), washed with 1 mL of DPBS, and again ultracentrifuged at 100,000×*g* for 1 h at 4 °C (TLA-55, BC). All pellets were re-suspended in 20 μL of radioimmunoprecipitation assay lysis buffer (RIPA) (1% IPEGAL CA-630 (Sigma-Aldrich), 0.1% sodium dodecyl sulfate (SDS), and 0.5% sodium deoxycholate in PBS (phosphate buffered saline)), supplemented with PIs, and frozen at − 20 °C until further use.

Immunoblot Analysis

To extract cell proteins, cells were lysed in RIPA buffer, supplemented with PIs for 15 min at 4 °C, and then centrifuged at 12,000×*g* for 15 min at 4 °C. The supernatant was collected and stored at − 20 °C for further use. Total protein concentration in samples was estimated with the BCA Protein Assay Kit (Thermo Fisher Scientific). Thirty micrograms of cell proteins, total fractionated cell proteins, or total EV proteins was separated by 12% SDS-polyacrylamide gel electrophoresis (SDS-PAGE) and transferred to a polyvinylidene fluoride (PVDF) membrane (Merck Milipore, Billerica, MA, USA). Mouse monoclonal antibodies against flotillin-I (610820, BD Bioscience, Oxford, UK), GAPDH (glyceraldehyde-3-phosphate dehydrogenase; G8795, Sigma-Aldrich), GFP (green fluorescent protein; sc-9996, Santa Cruz Biotechnology, Dallas, TX, USA), golgin-84 (611382, BD Bioscience), LAMP1 (lysosomal associated membrane protein 1; ab25630, Abcam, Cambridge, UK), PCNA (proliferating cell nuclear antigen; P8825, Sigma Aldrich), and TSG101 (protein encoded by tumor susceptibility gene; 4A10, Abcam); or goat polyclonal antibodies against annexin-II (sc-1924, Santa Cruz Biotechnology) and Rab7 (sc-6563, Santa Cruz Biotechnology); or rabbit polyclonal antibodies against calnexin (sc-11397, Santa Cruz Biotechnology) and CD63 (cluster of differentiation 63; sc-15363, Santa Cruz Biotechnology) were used as primary antibodies, and the appropriate HRP-conjugates anti-mouse, anti-goat, or anti-rabbit (Jackson ImmunoResearch Laboratories, West Grove, PA, USA) were used as the secondary antibodies. Membranes were developed by Luminata Forte Western HRP substrate (Merck Millipore) or SuperSignal West Pico Chemiluminescent Substrate (Thermo Fisher Scientific) and chemiluminescence detected on ImageQuant LAS-4000 (GE Healthcare, Buckinghamshire, UK). All antibodies were tested on the appropriate h-microglia cell lysates.

Solutions Used in Live Cell Microscopic Imaging

Extracellular solution (ECS) consisted of (in mM): 130 NaCl, 5 KCl, 2 $CaCl_2$, 1 $MgCl_2$, 10 D-glucose, and 10 HEPES (4-(2-hydroxyethyl)-1-piperazineethanesulfonic acid), pH 7.2 with NaOH. All chemicals were of the highest grade of purity available (Sigma-Aldrich). For stimulation, ionomycin solution was added to the ECS as a bolus to reach a final concentration of 2 μM. Similarly, the vehicle solution (DMSO) was added to ECS to reach a final concentration of 0.5‰ (*v*/*v*).

Cell Transfection and Fluorescent Labelling of Endocytotic Vesicles and Plasma Membrane in Live Cells

To visualize and examine the mobility of Nef.GFP puncta in h-microglia, cells were transfected with the pNef.GFP plasmid with Lipofectamine LTX (Thermo Fisher Scientific) according to the manufacturer's instructions. Briefly, DNA (~ 1 μg/μL) was mixed with 1 μL of Plus Reagent, diluted in 50 μL of

serum-free culture medium; 2 μL of Lipofectamine LTX Reagent was diluted in 50 μL of serum-free culture medium. Both solutions were mixed and incubated for 5 min at room temperature. Cells were then supplemented with 900 μL of serum-free culture medium, and 100 μL of the lipofection mixture was pipetted onto the cells. The cultures were incubated for 3 h at 37 °C in an atmosphere of 5% CO_2/95% air, and then 30 μL of Ultroser G (Pall Corporation, Port Washington, NY, USA) was added. The medium was exchanged for fresh culture medium the next day. Transfected cells were microscopically observed 48–72 h after transfection. The day before the onset of experiments, transfected cells were incubated overnight with 10 μM fluorescent dextran (Alexa Fluor-546 10,000 MW, D22911, Thermo Fisher Scientific) at 37 °C.

In a subset of experiments, acidic endo-/lysosomes were visualized in Nef.GFP-transfected, non-transfected, and mock-transfected cells (controls) by the addition of 200 nM of LysoTracker Red DND-99 (LyTR, Thermo Fisher Scientific) to the culture medium for 5 min at 37 °C. The LyTR was excited by a 561-nm diode-pumped solid-state (DPSS) laser line, and emission fluorescence was filtered with a band-pass filter 565–625 nm. In another subset of experiments, Nef.GFP-transfected cells were transferred into the recording chamber and supplied with 400 μL of ECS containing 4 μM FM4-64 (T3166, Thermo Fisher Scientific), which stained the plasma membrane and vesicles that internalized from the plasma membrane during endocytosis [29]. FM4-64 was excited by a 488-nm argon laser line and emission fluorescence was filtered with a band-pass filter 630–755 nm.

Immunocytochemistry and Fluorescence Co-localization Analysis

To examine the subcellular distribution of Nef.GFP structures in h-microglia, we quantified the fluorescence co-localization between Nef.GFP and immunocytochemically labelled proteins of plasma membrane or endosomal compartments (i.e., early endosomes, autophagosomes, late endosomes/lysosomes, MVBs). Transfected cells were washed (3 min) with PBS and fixed in formaldehyde (4% in PBS) for 15 min, permeabilized with 0.1% Triton X-100 for 10 min, and then washed four times with PBS at room temperature. The non-specific background staining was reduced by incubating cells in a blocking buffer with 10% (*v*/*v*) goat serum in PBS for 1 h at 37 °C. Then, cells were washed four times with PBS and incubated with primary antibodies diluted in 3% (*w*/*v*) bovine serum albumin (BSA) in PBS overnight at 4 °C. The following primary antibodies were used: rabbit polyclonal anti-GFP (green fluorescent protein; 1:200; AB3080, Merck Milipore), mouse monoclonal anti-CD9 (cluster of differentiation 9; 1:500; MCA469GT, Bio-Rad, Oxford, UK), mouse monoclonal anti-CD81 (cluster of differentiation 81; 1:200; NBP1-44861, Novus Biologicals, Bio-Techne, Oxon, UK), mouse monoclonal anti-TSG101 (protein encoded by tumor susceptibility gene; 1:100; ab83, Abcam, Cambridge, UK), mouse monoclonal anti-LC3 (microtubule-associated protein 1 light chain 3; 1:50; M152-3, MBL, Woburn, MA, USA), mouse monoclonal anti-EEA1 (early endosomal antigen 1; 1:100; 610456, BD Biosciences, Oxford, UK), and rabbit polyclonal anti-LAMP1 (lysosomal associated membrane protein 1; 1:300; Abcam, Cambridge, UK). Afterwards, the cells were washed in PBS (4 × 3 min) and stained with secondary anti-rabbit or anti-mouse antibodies conjugated to Alexa Fluor 546 (1:600; Thermo Fisher Scientific) at 37 °C for 45 min. Afterwards, the cells were washed in PBS (4 × 3 min) and mounted onto glass slides using SlowFade Gold antifade (Thermo Fisher Scientific). Double-fluorescent cells were observed with a confocal microscope (LSM 780; Zeiss, Jena, Germany) by a plan-apochromatic oil-immersion objective 63×/NA 1.4. Z-stacked images were obtained with a 488-nm argon laser and 561-nm DPSS laser excitation and the fluorescence emission was band-pass filtered at 495–530 and 565–625 nm, respectively.

In fixed cells, fluorescence co-localization between red-emitting fluorophores (immunofluorescent GFP, CD9, CD81, TSG101, LC3, EEA1, and LAMP1) and green-emitting Nef.GFP was quantified in 8-bit TIFF files exported to ColocAna software (Celica Biomedical, Ljubljana, Slovenia) [30]. The program summed up all pixels above the threshold in each channel (green, red) and pixels above the threshold in both channels (green and red). The threshold for the co-localized pixel count was set to 20% of the maximal fluorescence to minimize fluorescence overlap originating from closely positioned fluorescent structures (puncta) and structures above and below the focal plane that could contribute some out-of-focus light scatter. The fluorescence co-localization (%) of immunolabelled markers was determined with respect to the green Nef.GFP pixels. In double-fluorescent images of live cells, the co-localization of dextran-laden vesicles or FM4-64-stained plasma membrane (red) with Nef.GFP (green) fluorescence was quantified as stated above.

Vesicle Size Analysis

To estimate the apparent vesicle size (vesicle image area), confocal images of cells containing Nef.GFP structures and dextran-laden vesicles were analyzed with the ImageJ software (available at National Institute of Health, USA, http://rsbweb.nih.gov/ij/) after subtraction of background fluorescence (rolling ball radius 10 pixels). The minimum size of a fluorescent spot taken to identify an individual dextran-laden vesicle (or Nef.GFP-positive punctum) was three adjacent pixels (0.132 × 0.132 μm), and the minimum surface area covered by a punctum was 0.052 μm^2. This way,

a broad span of vesicles (puncta) with different apparent sizes was covered by the analysis.

Vesicle Mobility Analysis

Microglia-loaded coverslips were mounted into the recording chamber, supplied with 400 μL of ECS, and transferred to a confocal microscope (LSM 780; Zeiss) equipped with a plan-apochromatic oil-immersion objective 63×/NA 1.4. Nef.GFP was excited by a 488-nm argon laser line, and emission fluorescence was band-pass filtered with a filter 495–545 nm; fluorescent dextran was excited by a 561-nm DPSS laser line, and emission fluorescence was filtered with a band-pass filter 575–640 nm. Time-lapse images were acquired every ~ 0.5 s for 1 min before and 2 min after stimulation with 2 μM ionomycin (Iono). The mobility of Nef.GFP structures and dextran-laden vesicles was analyzed in exported tiff files with the ParticleTR software (Celica Biomedical, Ljubljana, Slovenia) [31]. Typically, ~ 35–50 randomly selected Nef.GFP-positive structures and/or dextran-laden vesicles were tracked per cell and the track length (TL; the pathway that individual vesicles travelled), the maximal displacement (MD; the farthest translocation of a vesicle), the directionality index (DI = MD/TL), and the speed were determined; all parameters were estimated for 15-s epochs. Analysis of the vesicle mobility was performed 1 min before and 2 min after the onset of cell stimulation with 2 μM ionomycin or application of the vehicle, 0.5‰ DMSO (*v*/*v*).

Nef.GFP Release Analysis

Nef release was estimated in individual cells by counting Nef.GFP-positive puncta in z-stacked confocal images acquired before and 1, 5, and 20 min after application of ionomycin or vehicle to the cells. For analysis, the background fluorescence was first subtracted (as stated above) and the number of Nef.GFP-positive puncta determined using 3D Object Counter plugin for ImageJ by considering that a given punctum consisted of at least three adjacent voxels. Time-dependent changes in Nef.GFP puncta number after application of ionomycin or vehicle to cells was expressed relative to the initial puncta number (as %).

Calcium Imaging and Analysis

Microglia-loaded coverslips were incubated for 30 min at room temperature in culture medium supplemented with 5 μM Fluo-4-AM, a cell-permeant fluorescent calcium indicator (Thermo Fisher Scientific). Then, cells were washed with ECS, incubated for 30 min to allow de-esterification of acetoxymethyl (AM) ester, and mounted into the chamber on a confocal microscope (LSM 780; Zeiss) equipped with a Plan-Apochromat air objective 20×/NA 0.8. Fluo-4 was excited by a 488-nm argon laser line and emission fluorescence was filtered with a 495–565 nm band-pass filter. Time-lapse images were acquired every second for 5 min before and 10 min after the bolus addition of ionomycin that reached a final concentration of 2 μM. The changes in Fluo-4 fluorescence, indicating changes in $[Ca^{2+}]_i$, were acquired by the Zen Black 2010 software (Zeiss) within the regions of interest that encompassed individual cells. The time-resolved fluorescence changes were analyzed by a custom written Matlab software (MathWorks, Natick, MA, USA) to obtain the peak calcium amplitude ($\Delta F/F_0$) and the surface under the curve (corresponding to the calcium amplitudes integrated over time ($\Delta F/F_0 \times t$)).

Statistical Analysis

The geometrical parameters (vesicle number, surface), parameters of vesicle mobility (TL, MD, DI, and speed), relative decrease in number of Nef.GFP structures, and parameters of calcium responses (peak and integrated increases in intracellular calcium concentration ($[Ca^{2+}]_i$)) were expressed as mean ± s.e. Statistical significance was determined with the Mann-Whitney *U* test or ANOVA on ranks using SigmaPlot 11.0 (Systat Software Inc., San Jose, CA, USA), and with ANCOVA using Matlab (MathWorks, Natick, MA, USA).

Results

Nef.GFP Separates into Subcellular Fractions Enriched with Organelles Immunopositive for Endosomal Proteins

Nef is released in the form of EVs from diverse Nef.GFP-expressing or HIV-1-infected cell types, but the subcellular origin of these EVs is not clear and is apparently cell type-dependent [16–18, 32, 33]. We here used cultured h-microglia as a model system to examine the cellular origin of Nef-containing EVs. Cells were first transfected with pNef.GFP or GFP (control), and after 48 h, the culture media and cells were separately collected for the immunoblot analysis. The culture medium was processed by ultracentrifugation following the protocol for EV isolation, and the pellet was analyzed by Western blotting for the presence of Nef.GFP (Fig. 1a, left). The pellet was immunopositive for Nef.GFP and for conserved vesicle proteins, such as flotillin and CD63. In the pellet obtained from the culture medium of GFP-expressing cells, GFP was also detected. Next we wanted to determine the subcellular origin of the released Nef.GFP. Thus, Nef.GFP-expressing h-microglia cultured for 48 h were homogenized and separated into four crude subcellular fractions: (i) the nuclear fraction (Nuc) containing nuclei, sheets of plasma membrane, and unbroken cells and debris; (ii) the light

mitochondrial fraction (LMF) containing mitochondria, lysosomes, peroxisomes, Golgi membranes, endoplasmic reticulum, and endosomes; (iii) the vesicle fraction (Ves) containing free cytoplasmic vesicles and microsomes; and (iv) the cytosolic fraction (Cyt) containing cytosolic proteins; differential centrifugation was performed as displayed in Fig. 1b. Next, we extracted proteins from collected fractions with RIPA buffer or TCA/DOC precipitation and analyzed them by Western blotting for the presence of Nef.GFP (Fig. 1c). Nef.GFP was enriched in the LMF fraction, which also tested immunopositive for the typical endo-lysosomal protein LAMP1, endoplasmic reticulum protein calnexin, and vesicle proteins annexin and flotillin. The specificity of the Nef.GFP subcellular localization to LMF is supported by the non-specific localization of GFP to all four subcellular fractions of the GFP-expressing h-microglia cells (Fig. 1c). The subcellular fractionation method was validated by the presence of PCNA in the crude nuclear fraction, GAPDH in the cytosolic fraction, and annexin and flotillin in the vesicle fraction. Since the obtained fractions were crude and could contain proteins typically associated with other organelles and fractions, we further separated the LMF fraction on a 15–25% iodixanol gradient (Fig. 1d). Proteins extracted by TCA/DOC from 17 collected subfractions were analyzed by Western blotting for the presence of Nef.GFP (Fig. 1d). Nef.GFP was detected in fractions 3–9, which overlapped with fractions immunopositive for the late endosomal protein Rab7 (fractions 6–8), endo-lysosomal protein LAMP1 (fractions 3–9), tetraspanin protein CD63 (fractions 3–5), endosomal sorting complexes required for transport (ESCRT) protein TSG101 (fractions 3–9), and membrane microdomain protein flotillin (fractions 3–9). Nef.GFP immunopositive fractions partly overlapped with fractions immunopositive for the Golgi apparatus protein golgin (fractions 6–10) but were mostly separate from the fractions immunopositive for the endoplasmic reticulum protein calnexin (fractions 15–17, weak signal 4–5). These results imply that before its release with EVs, Nef.GFP predominantly localizes to fractions enriched with compartments of endosomal origin in Nef.GFP-expressing h-microglia.

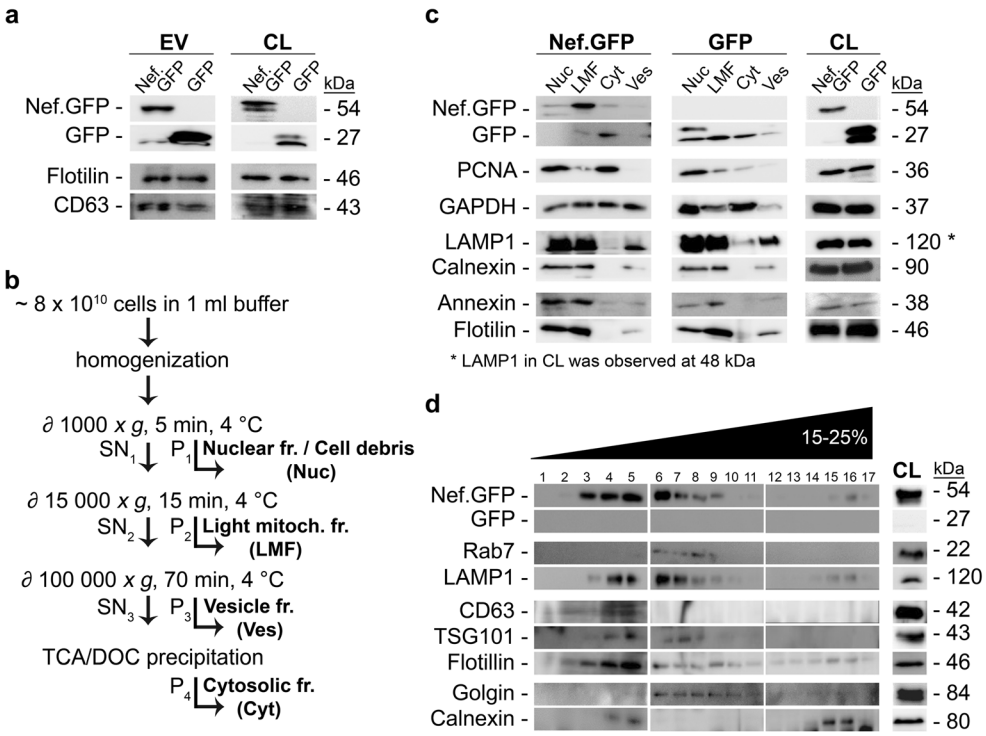

Fig. 1 Nef.GFP confines to gradient fractions immunopositive for endosomal proteins. **a** Protein composition of extracellular vesicles (EVs) isolated from Nef.GFP- and GFP-expressing h-microglia; CL cell lysate. Western blotting was performed with antibodies against GFP and markers for conserved vesicle proteins (flotillin, CD63). **b** Cell fractionation scheme. The partial differential symbol (∂) denotes centrifugation. For details, see the "Materials and Methods" section. SN supernatant, P pellet, TCA/DOC trichloroacetic acid and sodium deoxycholate. **c** Protein composition of the nuclear fraction that also contains cellular debris (Nuc), light mitochondrial fraction (LMF), cytosolic fraction (Cyt), and intracellular vesicles (Ves). Western blotting was performed with antibodies raised against GFP, markers for the nucleus (PCNA, proliferating cell nuclear antigen), cytosolic fraction (GAPDH), endo-/lysosomes (LAMP1), endoplasmic reticulum (calnexin), and conserved vesicle proteins (Annexin, flotillin). **d** Protein composition of the LMF fraction from Nef.GFP-expressing h-microglia separated on 15–25% iodixanol gradient. Western blotting was performed with antibodies raised against GFP, markers for late endosomes (Rab7), endo-/lysosomes (LAMP1), conserved vesicle proteins (CD63, TSG101, flotillin), Golgi (golgin), and endoplasmic reticulum (calnexin). CL cell lysate

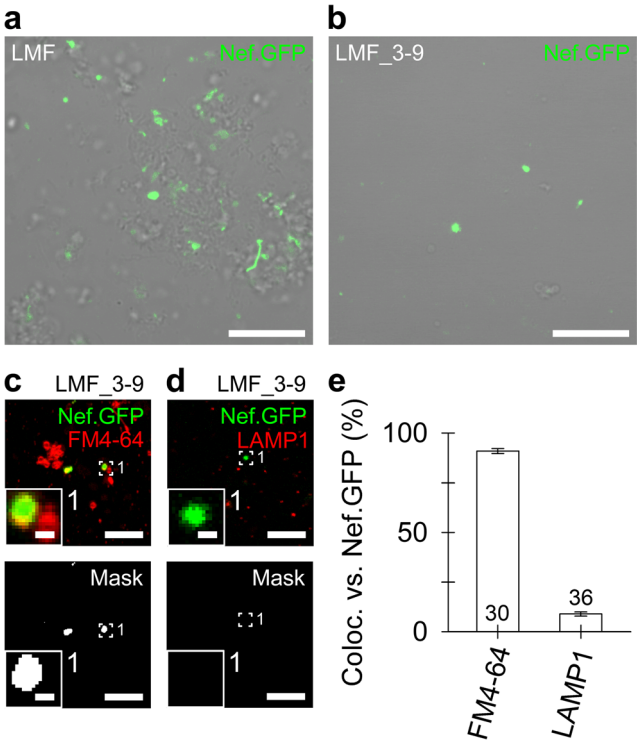

Fig. 2 Nef.GFP that confines to the light mitochondrial fraction structurally associates with membranous organelles distinct from late endosomes/lysosomes. **a**, **b** Combined differential interference contrast and confocal images of cellular organelles (visible as numerous translucent gray structures) and Nef.GFP-associated organelles (visible as green fluorescent puncta) from the light mitochondrial fraction (LMF; **a**) and the purified Nef.GFP-enriched LMF subfractions 3–9 (LMF_3–9 (**b**); see Fig. 1d). Note the less heterogeneous size and shape of Nef.GFP-positive structures in the LMF_3–9 compared to the crude LMF, indicative of a successful, density-based separation of organelles. **c**, **d** Nef.GFP in the LMF_3–9 predominantly associates with organelles stained with the styril membrane dye FM4-64 (**c**; fresh sample), but less with organelles immunopositive for LAMP1 (red) (**d**; fixed sample). Inset 1 (**c**) displays a magnified view of two FM4-64 labelled puncta (red) that are positive for Nef.GFP (left) or not (right). Inset 1 (**d**) displays a magnified view of the Nef.GFP structure that was not positive for immunofluorescently labelled LAMP1. The white mask images (**c**, **d**, bottom) display co-localized pixels; insets display magnified view of the selected structures (open frame). Scale bars: 10 μm (large images, **a**–**d**) and 0.5 μm (insets, **c**, **d**). **e** Graph displaying high fluorescence co-localization (mean ± s.e.; %) of FM4-64-stained organelles with Nef.GFP and low co-localization of immunofluorescent LAMP1 with Nef.GFP. The numbers at the bottom of the bars indicate the number of confocal images analyzed

Nef.GFP in the Light Mitochondrial Fraction Structurally Associates with Membranous Organelles Distinct from Late Endosomes/Lysosomes

Immunoblot data (Fig. 1d) suggested that Nef.GFP detected in LMF structurally associates with several membranous organelles of endosomal origin. Thus, we microscopically examined the crude LMF and the Nef.GFP-enriched fractions 3–9 of gradient-separated LMF (LMF_3–9) that were sealed to poly-L-lysine-coated coverslips. In the LMF, Nef.GFP was associated with diverse translucent cellular organelles of different sizes and shapes (Fig. 2a), whereas it was associated with morphologically less diverse organelles in the LMF_3–9 (Fig. 2b), evidencing successful organelle separation on the iodixanol density gradient (Fig. 1d). The addition of FM4-64 (10 μM) to the fresh LMF_3–9 revealed that Nef.GFP was associated with FM4-64-stained membranous organelles, which were more abundant than Nef.GFP-positive organelles (Fig. 2c, top). This indicates that Nef.GFP was associated with some, but not all, membranous organelles isolated in the LMF_3–9 (Fig. 2c, bottom). As further revealed by immunofluorescent labeling, Nef.GFP only minutely associated with LAMP1-positive organelles in the fixed LMF_3–9 (Fig. 2d, top and bottom). Correspondingly, the fluorescence co-localization between FM4-64 and Nef.GFP was high, 90.8 ± 1.3% (mean ± s.e.), whereas it was low, 8.9 ± 1.1%, between immunofluorescent LAMP1 and Nef.GFP (Fig. 2e). These data suggest that Nef.GFP predominantly associates with membranous organelles that differ from late endosomes/lysosomes in h-microglia.

Nef.GFP Structurally Associates with the Plasma Membrane-Derived Compartments and Is Spatially Segregated from Dextran-Laden Endo-/Lysosomes in Live H-Microglia

Since Nef.GFP associates with membranous organelles other than late endosomes/lysosomes in the LMF_3–9, we next examined to what extent Nef.GFP associates with the FM4-64-stained plasma membrane and dextran-laden endo-/lysosomes [34, 35] in live h-microglia (loaded overnight with fluorescent dextran (10 μM)). The fluorescence co-localization of both probes with Nef.GFP was calculated and compared to co-localization in positive controls immunofluorescently labelled with the anti-GFP antibody (Fig. 3a, top and bottom). The approach revealed ample fluorescence co-localization between FM4-64 and Nef.GFP structures (Fig. 3b, top and bottom) and scarce co-localization between dextran-laden vesicles and Nef.GFP structures (Fig. 3c, top and bottom). Specifically, fluorescence co-localization between FM4-64 and Nef.GFP structures was high, 66 ± 2%, although lower than in positive controls, 84 ± 2% (Fig. 3d). Notably, the fluorescence co-localization between dextran-laden vesicles and Nef.GFP structures was low, 9 ± 1% (Fig. 3d). Our data suggests that microglial Nef.GFP predominantly localizes to numerous, small plasma membrane-associated vesicle-like structures (puncta) that are spatially segregated from larger dextran-laden endo-/lysosomes localized in the perinuclear cytoplasmic cell region (Fig. 3c). This segregation was further

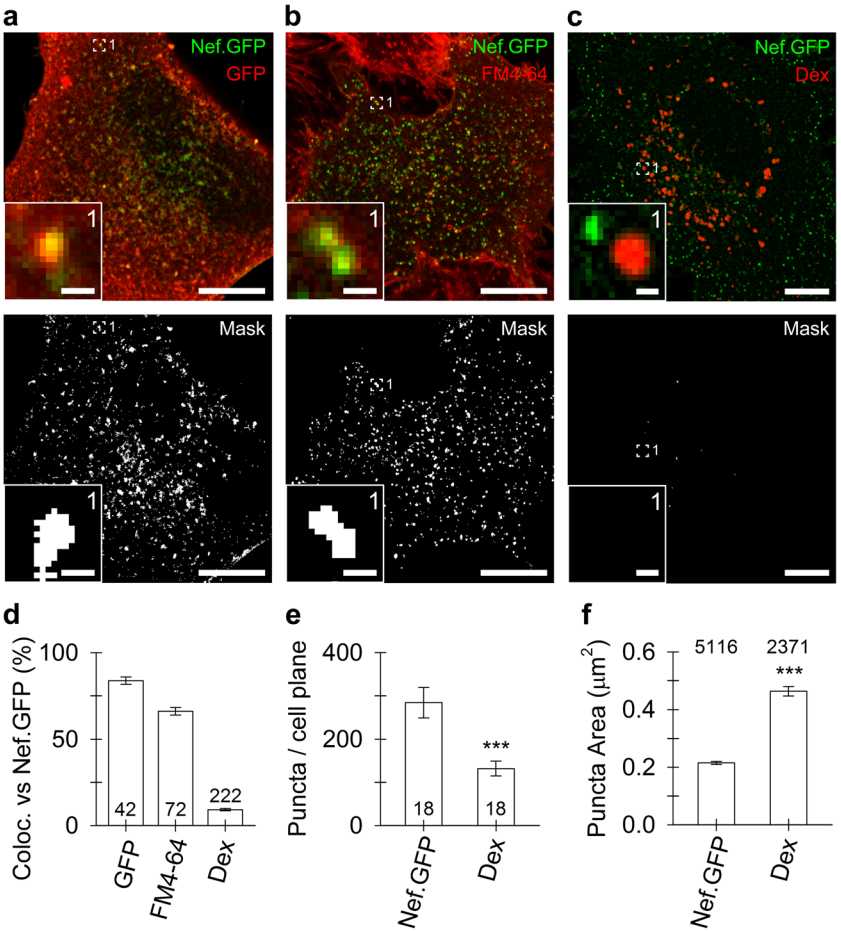

Fig. 3 Nef.GFP structurally associates with the plasma membrane-derived compartments and is segregated from dextran-laden vesicles in microglia. **a–c** Confocal images of transfected h-microglial cells expressing Nef.GFP (visible as green fluorescent puncta) labelled with the anti-GFP antibody and secondary Alexa546-conjugated antibody (red) (**a**; fixed cell), with the membrane styril dye FM4-64 (**b**; live cell), and with fluorescent dextrans that internalized into microglial vesicles (Dex) visible as large red puncta in the perinuclear cell region (**c**; live cell). Inset 1 displays a magnified view of the Nef.GFP structure immunofluorescently labelled with the anti-GFP antibody (**a**) and two Nef.GFP structures (puncta) labelled with FM4-64 (**b**). Inset 1 displays a magnified views of the region 1 (in **c**) where Nef.GFP structure did not co-localize (1) with dextran-laden vesicle. The white mask images display co-localized pixels (**a–c**, bottom), and insets display magnified view of the selected structures (open frame). Scale bars: 10 µm (large image) and 0.5 µm (insets) (**a–c**). **d** Quantitative co-localization (mean ± s.e.; %) of immunolabelled GFP, FM4-64, and dextran-laden vesicle fluorescence with Nef.GFP fluorescence. Note low fluorescence co-localization of dextran-laden vesicles with Nef.GFP structures. The numbers at the bottom of the bars indicate the number of cell images analyzed. **e**, **f** Quantitative comparison (mean ± s.e.) of the number of Nef.GFP-structures (puncta) and dextran-laden vesicles per cell plane (**e**) and vesicle area (**f**). The numbers at the bottom and top of the bars indicate the number of cell images and vesicles analyzed, respectively. ***$P < 0.001$ versus respective comparison (Mann-Whitney U test)

analytically confirmed by obtaining the counts and by comparing the size (surface area) of the imaged structures. The number (mean ± s.e.) of Nef.GFP structures exceeded the number of dextran-positive vesicles by > 2-fold (284 ± 35 vs. 132 ± 17, respectively; Fig. 3e), whereas the area of Nef.GFP-positive puncta was > 2-fold smaller than the area of dextran-laden endo-/lysosomes (0.21 ± 0.01 µm^2 vs. 0.46 ± 0.02 µm^2, respectively; Fig. 3f). These data suggest that intracellular Nef.GFP is segregated from dextran-laden endo-/lysosomes and predominantly associates with structures at the plasma membrane.

Nef.GFP Predominantly Localizes to the Plasma Membrane-Derived Compartments Immunopositive for Tetraspanins CD9 and CD81

Since Nef.GFP structures predominantly localized to plasma membrane-derived compartments and not to late endo-/lysosomal compartments in live h-microglia, we next examined their specific localization by quantifying the fluorescence co-localization between Nef.GFP structures and immunolabelled protein constituents of the plasma membrane and diverse endosomal compartments in fixed

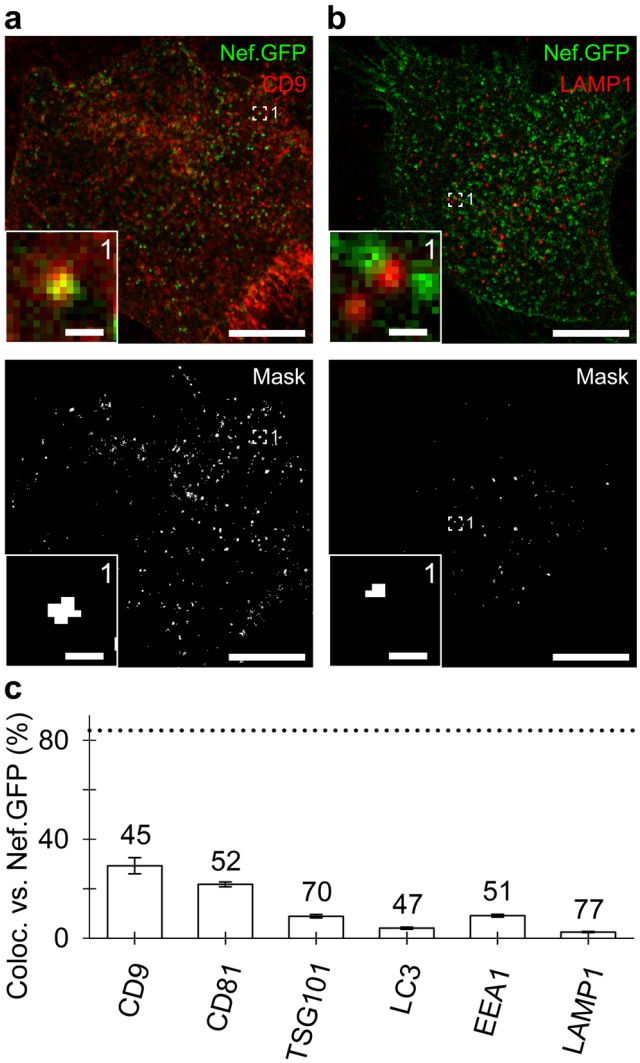

Fig. 4 Immunocytochemical characterization of Nef.GFP structures in h-microglia. **a**, **b** Confocal micrographs of fixed transfected h-microglial cells expressing Nef.GFP (green) labelled with the primary antibodies against CD9 (**a**) or LAMP1 (**b**) and the corresponding Alexa Fluor 546-conjugated secondary antibodies (red). Inset 1 (**a**) displays a magnified view of a Nef.GFP structure that co-localized with immunofluorescently labelled tetraspanin CD9, whereas inset 1 (**b**) displays a magnified view of a Nef.GFP structure that did not co-localize with immunofluorescently labelled LAMP1. The white mask images display co-localized pixels (**a**, **b**, bottom), and insets display magnified view of the selected structures (open frame). Scale bars: 10 μm (large images) and 0.5 μm (insets) (**a**, **b**). Note the different degrees of fluorescence co-localization between immunolabelled proteins and Nef.GFP in both micrographs. **c** Graph displaying quantitative co-localization (%, mean ± s.e.) of anti-CD9, anti-CD81, anti-TSG101, anti-LC3, anti-EEA1, and anti-LAMP1 fluorescence versus Nef.GFP fluorescence. The numbers above the bars indicate the number of cell images analyzed; the dotted black line indicates the mean fluorescence co-localization between anti-GFP and Nef.GFP (positive control). Note that Nef.GFP mostly co-localized with immunolabelled tetraspanins CD9 and CD81

transfected cells (Fig. 4a, b, top and bottom). The Nef.GFP structures were substantially immunopositive for the plasma membrane tetraspanins CD9 (36 ± 4%) and CD81 (22 ± 1%), weakly positive for the early endosomal protein EEA1 (9 ± 1%) and MVB protein TSG101 (9 ± 1%), and negligibly positive for the autophagosomal protein LC3 (4 ± 0%) and membrane protein of late endo-/lysosomes LAMP1 (2 ± 0%; Fig. 4c). These data suggest that Nef.GFP structures predominantly, but not exclusively, localize to plasma membrane-derived compartments, as suggested also by the optophysiological and biochemical data obtained in live and fractionated cells (Figs. 1, 2, and 3). We have also observed that the expression of Nef.GFP affects internalization of tetraspanin CD9 in Nef.GFP-expressing h-microglia. The relative amount of CD9 in the cell periphery (the thin peri-plasmalemmal space limiting the cell surface), compared to the central regions of the cell, was higher in non-transfected controls than in Nef.GFP-expressing h-microglia.

Nef.GFP Structures Display Retarded Mobility Characterized by Low Directionality

Since Nef.GFP apparently compartmentalized into numerous small vesicle-like structures in h-microglia, we next examined their mobility and compared it to mobility of dextran-laden vesicles in the same cells (Fig. 5a–d). The reconstructed tracks of Nef.GFP structures (see the "Materials and Methods" section for details) were stereotypically contorted (Fig. 5b) and indicated non-directional mobility (for detailed definitions, see [31]). In dextran-laden vesicles, the reconstructed vesicle tracks were more complex (elongated and contorted) and indicated both directional and non-directional vesicle motions (Fig. 5d), which differed from motions of Nef.GFP structures. Next, we performed a detailed mobility analysis of 1280 Nef.GFP-positive structures and 1140 dextran-laden vesicles in 8 cells, constructed frequency histograms, and fitted the data with logarithmic Gaussian functions (for details, see legend to Fig. 5e–g) to extract individual mobility parameters. In punctuated Nef.GFP (black bars), the vesicle track length (TL), maximal displacement (MD), and directionality index (DI) were distributed around the peak values of 1.29 ± 0.00 μm (Fig. 5e), 0.24 ± 0.00 μm (Fig. 5f), and 0.19 ± 0.00 (Fig. 5g), whereas in dextran-laden vesicles (white bars), they were distributed around the peak values of 1.88 ± 0.03 μm (Fig. 5e), 0.64 ± 0.02 μm (Fig. 5f), and 0.38 ± 0.01 μm (Fig. 5g), respectively. All mobility parameters were significantly diminished in Nef.GFP when compared to dextran-laden vesicles ($P < 0.001$). Next, we plotted the relationship between TL and MD of Nef.GFP structures and dextran-laden vesicles to estimate the fraction (%) of vesicles that maximally displace a distance > 1 μm within a 15 s epoch. The fraction of maximally displacing Nef.GFP puncta was insignificant (0.23%; Fig. 5h) in comparison to the fraction of maximally displacing dextran-laden vesicles (38.6%; Fig. 5i). The mobility of Nef.GFP structures thus exhibited little or no resemblance

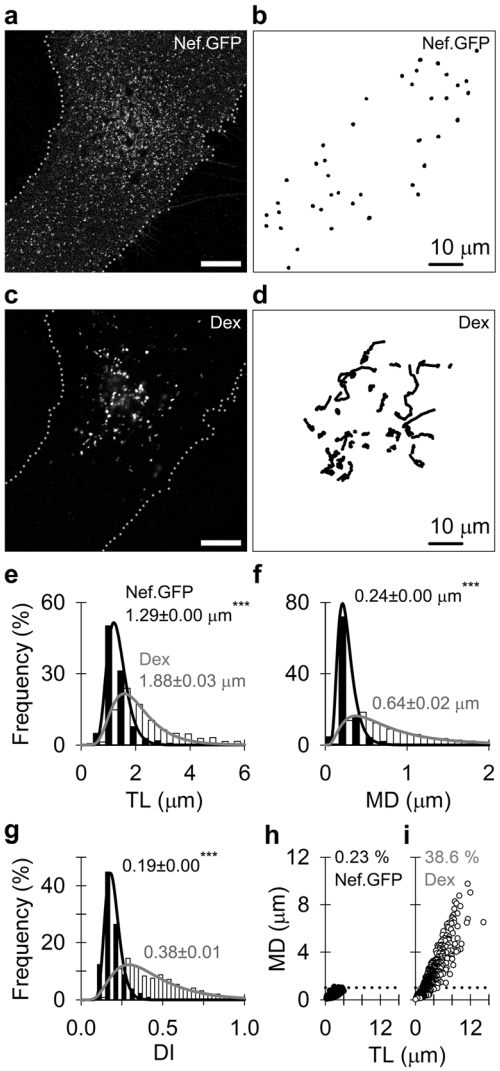

◀ **Fig. 5** Spontaneous mobility of Nef.GFP structures is smaller than mobility of dextran-laden vesicles in h-microglia. **a**, **c** Confocal micrographs of Nef.GFP-expressing h-microglial cell (**a**) containing dextran-laden vesicles (Dex) in the cytosol (**c**); scale bars, 10 μm. **b**, **d** Reconstructed tracks of Nef.GFP structures ($N = 40$) and dextran-laden vesicles ($N = 35$) in a 15-s epoch. Note that Nef.GFP structures displayed very limited mobility, as indicated by the highly contorted tracks (**b**), while many Dex vesicles displayed substantial mobility, as indicated by the elongated vesicle tracks (**d**). **e**–**g** Frequency histogram of the track length (TL; **e**), maximal displacement (MD, **f**), and directionality index (DI; **g**) obtained from Nef.GFP structures (1280 puncta in 8 cells, black histograms) and dextran-laden vesicles (1140 vesicles in 8 cells, white histograms). The data were fitted with the logarithmic Gaussian functions (Nef.GFP, black curve and Dex, gray curve) of the following form: $f = a*\exp(-0.5 \times (x/x_0)/b)^2/x$, whereby $a = 64.24 \pm 0.52$, $b = 0.27 \pm 0.00$ $\mu m^{-0.5}$, $x_0 = 1.29 \pm 0.00$ μm (Nef.GFP) and $a = 37.34 \pm 1.25$, $b = 0.42 \pm 0.02$ $\mu m^{-0.5}$, $x_0 = 1.88 \pm 0.03$ μm (Dex) in TL data (**e**); $a = 17.98 \pm 0.09$, $b = 0.39 \pm 0.00$ $\mu m^{-0.5}$, $x_0 = 0.24 \pm 0.00$ μm (Nef.GFP) and $a = 7.99 \pm 0.21$, $b = 0.73 \pm 0.02$ $\mu m^{-0.5}$, $x_0 = 0.64 \pm 0.02$ μm (Dex) in MD data (**f**); and $a = 8.19 \pm 0.14$, $b = 0.23 \pm 0.00$ $\mu m^{-0.5}$, $x_0 = 0.19 \pm 0.00$ (Nef.GFP) and $a = 4.04 \pm 0.21$, $b = 0.51 \pm 0.03$ $\mu m^{-0.5}$, $x_0 = 0.38 \pm 0.01$ (Dex) in DI data (**g**). **h**, **i** Plots displaying the relationship between MD and TL in spontaneously mobile Nef.GFP structures (black circles) and dextran-laden vesicles (white circles). Strongly displacing vesicles with MD > 1 μm (above the dashed line, with the corresponding percentage) and weakly displacing vesicles with MD < 1 μm are displayed. Note the negligible proportion of strongly displaced Nef.GFP structures in comparison to dextran-laden vesicles

to the mobility of dextran-laden vesicles. These two structures appear to be transported by fundamentally different cellular mechanisms.

Expression of Nef.GFP Hampers Mobility of LysoTracker-L Vesicles in H-Microglia

Despite obvious differences in the cytoplasmic mobility of Nef.GFP structures and dextran-laden endosomes, the intracellular trafficking of endocytotic organelles can be modified by the expression of Nef itself [36]. Thus, we also examined how the expression of Nef.GFP affects the mobility of LysoTracker (LyTR)-laden vesicles (that predominantly constitute endo-/lysosomes with an acidified lumen [37]) in h-microglia (Online Resource 1). For this purpose, spontaneous mobility of LyTR-laden vesicles ($N = 5402$) was analyzed in non-transfected cells ($N = 11$; Online Resource 1a), in cells exposed to transfection agents devoid of added pNef.GFP (mock-transfected; $N = 9$) and in pNef.GFP-transfected cells ($N = 11$; Online Resource 1b). When compared to non-transfected controls, the TL, MD, DI, and speed were reduced significantly ($P < 0.001$ or $P < 0.05$) by ~ 24, ~ 30, ~ 7, and ~ 24% in Nef.GFP-expressing cells (Online Resource 1c–f), but not in mock-transfected cells (Online Resource 1c–f). These data suggest that trafficking of acidified endo-/lysosomes is impaired in Nef.GFP-expressing h-microglia.

Ionomycin Stimulation Elevates Intracellular Calcium Activity and Irrecoverably Attenuates Mobility of Dextran-Laden Vesicles, but Not of Nef.GFP Structures

Next, we examined whether alterations in h-microglial calcium homeostasis affect the mobility of Nef.GFP structures and dextran-laden vesicles as previously observed in different types of gliotransmitter-loaded vesicles [35, 37–39]. Changes in $[Ca^{2+}]_i$ were examined with microfluorimetry in h-microglia loaded with the fluorescent Ca^{2+} indicator Fluo-4 (Fig. 6a, left). Application of 2 μM ionomycin to cells evoked robust and prolonged increases in $[Ca^{2+}]_i$ (Fig. 6a, middle and right and Fig. 6b, top), in contrast to application of vehicle (0.5‰ DMSO (*v*/*v*); Fig. 6b, bottom). Stimulus-evoked changes in $[Ca^{2+}]_i$ were quantified by measuring the normalized peak amplitudes (p, $\Delta F/F_0$) and the time integral in $[Ca^{2+}]_i$ (S, $\Delta F/F_0 \times s$) (Fig. 6b, top). In vehicle-treated controls ($n = 73$), the peak (p) values in $[Ca^{2+}]_i$ were negligible, whereas application of 2 μM ionomycin to cells ($N = 77$) evoked a significant increase in p $[Ca^{2+}]_i$ ($P < 0.001$) (Fig. 6c).

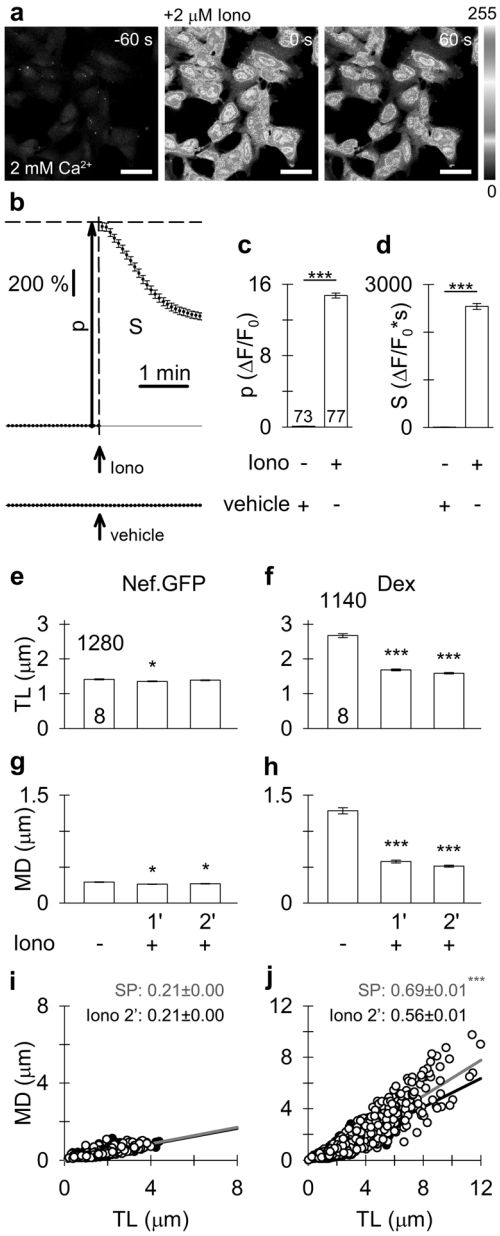

◀ **Fig. 6** Ionomycin stimulation transiently elevates intracellular calcium activity and suppresses directional mobility of dextran-laden vesicles, but not of Nef.GFP structures. **a** Confocal micrographs of fluorescent Ca^{2+} indicator Fluo-4 loaded in h-microglia before (− 60 s, left) and after stimulation with 2 μM ionomycin (Iono) to increase intracellular calcium activity (60 s (middle) and 120 s (right) after application of Iono). Ionomycin evoked large increases in intracellular calcium activity as indicated by the intensity grayscale levels (right, 0–255 intensity levels). Scale bars: 50 μm. **b** Time-resolved ionomycin-evoked changes in $[Ca^{2+}]_i$ were quantified by determining the peak $[Ca^{2+}]_i$ (*p*, mean ± s.e.) relative to the baseline fluorescence (gray horizontal line, F_0) and the time-integrated $[Ca^{2+}]_i$ (*S*) evoked by 2 μM ionomycin (Iono) or 0.5‰ DMSO (*v*/*v*) (vehicle). **c**, **d** The peak (*p*) and the time-integrated calcium responses (*S*) evoked by application of Iono or vehicle to cells. Iono (+) mobilized large amount of Ca^{2+} into the cytosol of h-microglia, whereas vehicle (+) did not elevate calcium activity. The numbers at the bottom of the bars indicate the number of cells analyzed. $***P < 0.001$ versus respective comparison (Mann-Whitney *U* test). **e**–**h** Mobility of Nef.GFP structures and dextran-laden vesicles (**e**, **f**, TL; **g**, **h**, MD; mean ± s.e.) before (−) and within the first (1′) and second (2′) minute after ionomycin stimulation. Note the strong ionomycin-evoked reduction in mobility of dextran-laden vesicles, but not of Nef.GFP structures. The numbers at the top and bottom of the bars indicate the number of vesicles (puncta) and cells analyzed, respectively. $*P < 0.05$, $***P < 0.001$ versus non-stimulated mobility (ANOVA on ranks followed by Tukey's test). (**i**, **j**) Plots displaying the relationship between MD and TL in Nef.GFP structures and dextran-laden vesicles before stimulation (**i**, **j**, white circles) and during the second minute (**i**, **j**, black circles) after ionomycin stimulation. A linear function of the form $[MD = MD_0 + a \times (TL)]$ was fitted to the data (gray and black lines; before and after Iono stimulation) to obtain slopes indicating the directionality of mobility. In the second post-stimulation minute, the slope (a ± s.e.; displayed above the graphs) diminished significantly in dextran-laden vesicles, but not in Nef.GFP structures ($***P < 0.001$; ANCOVA)

Correspondingly, the mobilization of free Ca^{2+} measured as 2-min time integral (*S*) was negligible in controls, whereas the application of ionomycin resulted in a substantial increase in *S* (Fig. 6d).

Thereafter, the time-and Ca^{2+}-dependent changes in mobility (TL and MD) of Nef.GFP structures and dextran-laden vesicles were recorded for 1 min before and 2 min after cell stimulation with ionomycin and compared with data obtained prior to stimulation. The post-stimulation data were subdivided into the first and second post-stimulation minute. Ionomycin barely affected TL in Nef.GFP structures (Fig. 6e), predominantly due to smaller initial resting values, along with a similar "leveling" in the ionomycin-evoked reduction of mobility. In dextran-laden vesicles, however, ionomycin stimulation evoked a strong and sustained reduction in TL (Fig. 6f), which decreased by 37 and 41% during the first and second post-stimulation minutes, respectively. In Nef.GFP structures, MD decreased minutely, but significantly ($P < 0.05$), by 10% during the first and by 8% during the second post-stimulation minute (Fig. 6g), respectively. In dextran-laden vesicles, MD decreased profoundly ($P < 0.001$), by 55% and by 60% during the first and second post-stimulation minute (Fig. 6h), respectively. In addition, we examined the effect of ionomycin stimulation on the directionality of vesicle motions by fitting a linear function $[MD = MD_0 + a \times (TL)]$ to the data. In Nef.GFP structures, TL and MD exhibited little or no change during the entire post-stimulation period; thus, no decrease in the slope (a) was observed (Fig. 6i). In dextran-laden vesicles, the slope (a) significantly decreased ($P < 0.001$) from 0.69 ± 0.01 before stimulation to 0.56 ± 0.01 during the second post-stimulation minute (Fig. 6j), which indicated a Ca^{2+}-dependent reduction in directional mobility of dextran-laden vesicles. Collectively, these data indicate that mobility of Nef.GFP structures and endo-/lysosomes is differentially regulated by altered h-microglial calcium homeostasis. During acute ionomycin stimulation, neither Nef.GFP structures nor dextran-laden vesicles displayed any

tendency for mobility recovery (0–120 s) (Online Resource 2) suggesting a debilitating impact of elevated $[Ca^{2+}]_i$ on vesicle mobility in h-microglia.

Slow Spontaneous Release of Nef.GFP from H-Microglia Is Inhibited by Ionomycin Stimulation

Finally, we examined whether elevated $[Ca^{2+}]_i$ also evokes release of Nef.GFP structures from h-microglia, indicative of EV release [16]. In time series of confocal images acquired 1 min before and 2 min after application of ionomycin, we could not detect any sudden, step-wise changes in puncta fluorescence resembling exocytotic cargo release from individual vesicles [40, 41] (data not shown). Thus, we next acquired confocal z-stacked images of individual cells before and 1, 5, and 20 min after the application of ionomycin (2 μM) or vehicle (0.5‰ DMSO (*v*/*v*) to (i) visualize Nef.GFP structures distributed throughout the entire vertical (z) profile and (ii) to increase the probability of detecting an individual release event. In 3D reconstructed images obtained in cells exposed to ionomycin (Fig. 7a) or vehicle (Fig. 7b), we could observe numerous Nef.GFP structures at the onset and at the end of treatment (after 20 min). The detailed analysis revealed that the relative number of Nef.GFP structures (expressed as percentage of initial number) decreased significantly ($P < 0.05$) from 100 to 91.5 ± 2.45% after 20 min in vehicle-treated controls, but not in ionomycin-stimulated cells (Fig. 7c). Next, we examined the rate of Nef.GFP structures (puncta) reduction by fitting a linear function $[y = y_0 + a \times (x)]$ to these data. In ionomycin-stimulated cells, the relative puncta number did not change during the post-stimulation period (Fig. 7d, black line). In vehicle-treated controls, however, the relative puncta number significantly decreased and the function slope ($a = -0.4 \pm 0.0$%/min) significantly differed ($P < 0.05$) from the slope of ionomycin-stimulated cells ($a = 0.0 \pm 0.1$%/min). These data suggest that Nef.GFP structures are slowly, but significantly released from h-microglia; surprisingly, their release is inhibited by increased h-microglial free calcium level.

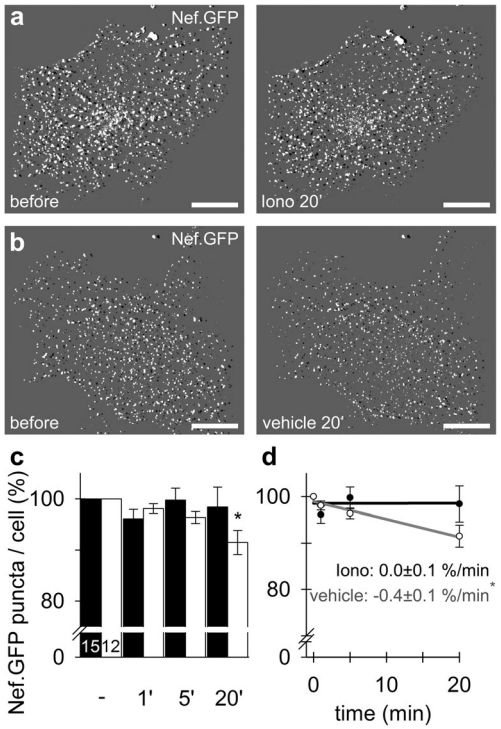

Fig. 7 Ionomycin stimulation inhibits the slow time-dependent decrease in the number of Nef.GFP structures in h-microglia. (**a, b**) Three-dimensional shaded display of Nef.GFP structures observed before (left) and 20 min after (right) application of 2 μM ionomycin (Iono) (**a**) or vehicle (0.5‰ DMSO (*v*/*v*)) to cells (**b**). In the ionomycin-stimulated cell, the number of Nef.GFP puncta (white) decreased less (from 1094 to 1051, ~ 3.9%; **a**) than in the vehicle-treated cell (from 952 to 880, ~ 7.6%; **b**). Scale bars, 10 μm. (**c**) The relative decrease (mean ± s.e.; %) in the number of Nef.GFP puncta observed 1, 5, and 20 min after application of ionomycin (black bars) or vehicle to cells (white bars). The numbers at the bottom of the bars indicate the number of cells analyzed. *$P < 0.05$ versus initial puncta number (ANOVA on ranks followed by Tukey's post hoc test). **d** Plot displaying the rate of Nef.GFP structures reduction in ionomycin-stimulated cells (black circles) and control cells (white circles). A linear function of the form $y = y_0 + a \times (x)$ was fitted to the data (black line, Nef.GFP and gray line, Dex) to obtain the slope ($a \pm$ s.e.; displayed in graph), which reports the rate of puncta reduction over time; the slope was significantly decreased in controls versus ionomycin-stimulated cells (*$P < 0.05$; ANCOVA)

Discussion

Nef.GFP Predominantly Localizes to the Plasma Membrane-Derived Compartments Immunopositive for Tetraspanins CD9 and CD81 in H-Microglia

This study is the first to characterize the subcellular compartmentalization of the HIV protein Nef, examine its intracellular mobility, and investigate Nef release dynamics from single cultured human microglia. To examine the intracellular distribution of Nef (Fig. 1a), Nef.GFP was expressed in cultured human microglia (h-microglia). The distinct punctuated pattern of Nef.GFP fluorescence indicated its widespread cellular distribution that seemingly originates from the ability of myristoylated Nef to associate with membranous organelles [42] (Fig. 2c) and with the plasma membrane (Fig. 3b), as reported in Nef.GFP-expressing human HeLa cells [43]. Immunoblot analysis of subcellular fractions (Fig. 1c, d) indicated the association of Nef.GFP with membranous organelles, as it separated into iodixanol gradient fractions with similar buoyant density as organelles immunopositive for endo- and lysosomal protein LAMP1 and to a certain extent also for late endosomal protein Rab7, tetraspanin CD63, ESCRT protein TSG101, and membrane microdomain protein

flotillin (Fig. 1d). The detailed microscopic analysis of fluorescently labelled organelles isolated from Nef.GFP-positive gradient fractions and intact Nef.GFP-expressing cells revealed that Nef.GFP structures only marginally co-localized with immunolabelled protein markers of lysosomes (Fig. 2d, e), MVBs, and endo-/lysosomes (Fig. 4). Similarly, Nef.GFP structures only minutely co-localized with endo-/lysosomes (Fig. 3d) accumulating fluorescent dextrans [44] or with acidified [37] LysoTracker-laden vesicles (data not shown), indicating that membrane-associated Nef.GFP structures were unlikely part of the endosomal system and did not have an acidified lumen. The Nef.GFP-associated small vesicle-like structures differed from endo-/lysosomes also in terms of abundance, size (area) (Fig. 3e, f), and intracellular trafficking (Figs. 5 and 6). On the other side, numerous Nef.GFP puncta co-localized with organelles immunopositive for tetraspanins CD9 and CD81 (Fig. 4). Similar was observed in monocyte-derived macrophages (MDM), where immunofluorescence staining indicated that CD81, CD9, and CD53 are present at the plasma membrane and also in a population of intracellular puncta that differ from EEA1-containing early endosomes or the tubulovesicular late endosomes/lysosomes marked by CD63 and LAMP1 [45]. Thus, it seems that in intact h-microglia, Nef.GFP mostly associates with the plasma membrane-derived compartments.

Several recent studies have described a novel cellular compartment in monocyte-derived macrophages (MDMs), termed the virus-containing compartment (VCC) or the intracellular plasma membrane-connected compartment (IPMC) [46], with some characteristics similar to the h-microglial Nef.GFP structures observed in this study. IPMCs have (i) a complex three-dimensional morphology and some resemble MVBs, while others consist of closely apposed membranes or interconnected sponge-like membranes [45]; (ii) a unique set of protein markers, like tetraspanins CD81, CD9, and CD53 [45] and proteins clustered at the coated domains (β2, αM, αX integrins, talin, vinculin, paxillin) [47]; (iii) near-neutral pH [48]; and (iv) some have connections to the extracellular milieu via narrow channels but are largely inaccessible to antibodies, cationized ferritin, or dextran [49]. IPMCs develop in MDMs after HIV-1 infection, as the cells differentiate and become further enlarged, and serve as sites of virus assembly and accumulation [47, 50]. Interestingly, HIV-1 infection stimulates early autophagy in macrophages, but Nef inhibits autophagic maturation, thereby preventing fusion with lysosomes and possibly promoting fusion with IPMCs [51]. Additionally, Nef upregulates tetherin in HIV-1-infected MDMs, which localizes to IPMCs and possibly physically tethers virions to the limiting membranes of the compartment [49]. Similar roles for Nef in connection to IPMCs could be envisioned in Nef.GFP-expressing h-microglia.

Apart from association with membranous organelles, the punctuated Nef.GFP fluorescence could also originate from the self-association properties of Nef, resulting in the formation of oligomeric or even polymeric non-covalently associated Nef forms. Oligomerization of biological polypeptides is a common mechanism used to trigger events in cellular signaling and endocytosis, both of which are targeted by Nef [9, 36]. However, the formation of higher Nef.GFP oligomers appears unlikely, since the Nef core domain forms stable homo-dimers and trimers, but not oligomers, in solution [52]. Moreover, we also observed high co-localization of Nef.GFP with FM4-64-stained plasma membrane structures (Fig. 3b, d), suggesting that compartmentalization of Nef.GFP is more likely due to the association of Nef with the aforementioned membranes of h-microglia. Studies in liposomes have suggested that the association of myristoylated Nef strongly depends on the negative net charge of liposomes [42]. No Nef binding occurs in uncharged liposomes and the kinetics of Nef membrane association strongly depends on the membrane curvature of liposomes. The smallest microglial vesicles are thus the likeliest candidates for Nef.GFP binding, since the increased positive curvature in these vesicles likely spreads lipids apart in the convex leaflet of the membrane, allowing easier insertion of the myristate. Moreover, Nef itself is able to induce membrane deformation and formation of highly curved (small) vesicles [42], which were consistently observed in our study as well as in others [7, 43].

The Mobility of Nef Structures Is Governed by a Different Mechanism than the Mobility of Dextran-Laden Vesicles in H-Microglia

Besides the differences between Nef.GFP structures and dextran-laden vesicles in h-microglia (Fig. 3), the former also displayed limited mobility, characterized by pronounced non-directionality (Fig. 5). The mobility patterns of Nef.GFP structures essentially indicated that their trafficking is more likely governed by diffusion than by the cytoskeleton-dependent mechanism(s) in which motor proteins propel vesicles [53] over distances of several micrometers without dissociating from the cytoskeletal tracks. The low directional mobility ($DI = 0.19 \pm 0.00$) renders Nef.GFP structures unlikely to be quickly delivered towards any particular cellular location, except for the most proximal ones ($MD < 1$ μm). Similarly reduced and pronounced non-directional vesicle mobility was observed in astrocytes treated with the microtubule- and actin-depolymerizing agents nocodazole and Clostridium spiroforme toxin [54]. In striking contrast to Nef.GFP structures, dextran-laden vesicles displayed more complex mobility composed of forward and backward motions interrupted by periods of arrested mobility in h-microglia, as previously reported in endosomes containing low-density lipoproteins [55], LysoTracker-laden [38], and dextran-laden astroglial vesicles [35]. The mobility of fast directional dextran-laden vesicles in

h-microglia corresponded well to the cytoskeleton-dependent vesicle mobility observed in astrocytes [38, 39, 41, 54].

Of note is also that ionomycin stimulation of h-microglia evoked substantial diminishment in the mobility of dextran-laden vesicles, but not of Nef.GFP structures (Fig. 6e–h). The significant reduction in directional mobility of dextran-laden vesicles, but not of Nef.GFP structures (Fig. 6i, j), may indicate that dextran-laden endo-/lysosomes were temporarily disconnected from the cytoskeleton and subjected to only Brownian motion. Alternatively, the structural integrity of the cytoskeletal trafficking substrate was compromised by the ionomycin-evoked elevation in $[Ca^{2+}]_i$ (Fig. 6a–d), which is known to impact cytoplasmic translocation of lysosomes by modulating microtubule polymerization and depolymerization [56]. In vitro, polymerization of isolated tubulin is blocked in solutions containing 6 μM Ca^{2+} [57], whereas induction of microtubule fragmentation or depolymerization begins at ~ 1–100 μM $[Ca^{2+}]$ [58, 59]. In vivo, similar $[Ca^{2+}]_i$ elicit similar effects on microtubules, with microtubule-associated proteins shifting the effective $[Ca^{2+}]$ upwards [60]. Since the mobility of dextran-laden vesicles irrecoverably diminished during acute ionomycin stimulation of h-microglia (Online Resource 2), partial disassembly of microtubules appears more likely than transient disconnection of mobile vesicles from the microtubule cytoskeleton. Notably, diffusion of Ca^{2+} through the cytoplasm likely produces a pattern of microtubule disassembly proceeding from the periphery to the cell center [59].

Expression of Nef.GFP in H-Microglia Diminishes Mobility of Acidified LyTR-Laden Vesicles

As further revealed, Nef.GFP expression in h-microglia significantly hampered the mobility of LyTR-laden vesicles (Online Resource 1), which may indicate compromised intracellular sorting/handling of material targeted for degradation or lysis in lysosomes/autophagolysosomes [61]. The later may form during macroautophagy, a multistep catabolic process through which cytoplasmic material, including long-lived proteins, aggregated proteins, and dysfunctional organelles, are delivered to the lysosome for degradation [62]. In accordance with the compromised mobility of lysosomes, infection of human microglia with HIV-1_{SF162} resulted in increased levels of microtubule-associated protein 1 light chain 3 (LC3), suggesting that HIV-1 infection triggered autophagosome formation without promoting lysosomal protein degradation. Similarly, the expression of Nef in primary human fetal astrocytes compromised the autophagic pathway by inducing autophagosome formation and blocking the assembly of autophagolysosomes [63]. Moreover, the autophagy-related proteins LC3 and Beclin 1 were found in complexes with the HIV-1 proteins Gag and Nef in macrophages, providing a basis for Nef function in controlling autophagy [51]. By using the RFP-GFP-LC3 probe, which helps discriminate non-degradative autophagosomes from degradative autophagolysosomes based on probe sensitivity to pH [64], it was possible to demonstrate that Nef blocked maturation of early autophagosomes into acidified, degradative autophagolysosomes. Since the effects of Nef on autophagy are predominantly based on blocking autophagic flux, retarded mobility of lysosomes in Nef-expressing cells corroborates these findings and adds another level of regulation of autophagolysosome formation. It is possible that Nef acts as a multifaceted player in the dysregulation of autophagy in Nef-expressing cells.

Altered Calcium Homeostasis Inhibits Slow Nef.GFP Release from H-Microglia

Several in vitro studies have indirectly demonstrated that Nef.GFP-transfected or HIV-infected cells release Nef in the form of EVs [16, 17, 25, 65]. Moreover, Nef released from HIV-infected cells was detected in the plasma of HIV+ individuals [18, 32]. We have similarly demonstrated that Nef.GFP is released from h-microglia, most likely in a membrane-bound form. Nef.GFP was detected in the culture media pellet immunopositive for the typical EV proteins flotillin and CD63 (Fig. 1a), which was obtained by the use of a standard ultracentrifugation procedure for EV isolation [66]. Apart from the biochemical analysis of the particles pelleted from the culture media, we also estimated the rate of Nef.GFP release from individual microglial cells (Fig. 7). The rate of ~ 0.4% Nef.GFP structures per min indicated slow, but continuous release from cells (Fig. 7d). By assuming that constant Nef release is not counterbalanced by de novo formation of EV-like structures, the entire cellular pool of Nef structures is expected to be depleted within ~ 4 h. Interestingly, cell stimulation with ionomycin inhibited rather than facilitated Nef release, indicating that the microglial mechanism of Nef release does not resemble calcium-dependent vesicle exocytosis in glia [67]. These results also support the view that Nef.GFP structures only marginally localized to lysosomes that are prone to calcium-dependent exocytotic release of luminal cargo [68]. Instead, Nef apparently stimulates its own release from h-microglia through the production of abundant EV-like structures associated with plasma membrane-derived compartments. If a similar release occurs in vivo, surrounding neurons may take up Nef-positive EVs and consequently undergo oxidative stress [25] that contributes to the neurotoxicity observed in HIV-1-infected AIDS patients [69]. In conclusion, this study is the first to report that plasma membrane-derived compartments act as sites of Nef-positive extracellular vesicle biogenesis and release.

Acknowledgements We thank Ms. Ana Gabrovec for assistance in image analysis. We kindly thank Prof. Jonathan Karn for sharing h-microglia cells and Profs. Peter Veranič and Tea Lanišnik Rižner for sharing antibodies.

Funding Information The authors acknowledge the financial support from the Slovenian Research Agency (research core funding #P3 310, and the projects J3-5499, J3-3632, J3-4051, J3-4146, J3-6790, P1-170.

Compliance with Ethical Standards

Conflict of Interest The authors declare that they have no conflict of interest.

References

1. Chompre G, Cruz E, Maldonado L, Rivera-Amill V, Porter JT, Noel RJ Jr (2013) Astrocytic expression of HIV-1 Nef impairs spatial and recognition memory. Neurobiol Dis 49:128–136. https://doi.org/10.1016/j.nbd.2012.08.007
2. Si Q, Kim MO, Zhao ML, Landau NR, Goldstein H, Lee S (2002) Vpr- and Nef-dependent induction of RANTES/CCL5 in microglial cells. Virology 301(2):342–353
3. Kaul M, Lipton SA (2006) Mechanisms of neuronal injury and death in HIV-1 associated dementia. Curr HIV Res 4(3):307–318
4. Hanna Z, Kay DG, Rebai N, Guimond A, Jothy S, Jolicoeur P (1998) Nef harbors a major determinant of pathogenicity for an AIDS-like disease induced by HIV-1 in transgenic mice. Cell 95(2):163–175
5. Foti M, Cartier L, Piguet V, Lew DP, Carpentier JL, Trono D, Krause KH (1999) The HIV Nef protein alters Ca(2+) signaling in myelomonocytic cells through SH3-mediated protein-protein interactions. J Biol Chem 274(49):34765–34772
6. Brigino E, Haraguchi S, Koutsonikolis A, Cianciolo GJ, Owens U, Good RA, Day NK (1997) Interleukin 10 is induced by recombinant HIV-1 Nef protein involving the calcium/calmodulin-dependent phosphodiesterase signal transduction pathway. Proc Natl Acad Sci U S A 94(7):3178–3182
7. Bentham M, Mazaleyrat S, Harris M (2006) Role of myristoylation and N-terminal basic residues in membrane association of the human immunodeficiency virus type 1 Nef protein. J Gen Virol 87 (Pt 3):563–571. doi:https://doi.org/10.1099/vir.0.81200-0
8. Breuer S, Gerlach H, Kolaric B, Urbanke C, Opitz N, Geyer M (2006) Biochemical indication for myristoylation-dependent conformational changes in HIV-1 Nef. Biochemistry 45(7):2339–2349. https://doi.org/10.1021/bi052052c
9. Geyer M, Fackler OT, Peterlin BM (2001) Structure-function relationships in HIV-1 Nef. EMBO Rep 2(7):580–585. https://doi.org/10.1093/embo-reports/kve141
10. Marsh JW (1999) The numerous effector functions of Nef. Arch Biochem Biophys 365(2):192–198. https://doi.org/10.1006/abbi.1999.1208
11. Madrid R, Janvier K, Hitchin D, Day J, Coleman S, Noviello C, Bouchet J, Benmerah A et al (2005) Nef-induced alteration of the early/recycling endosomal compartment correlates with enhancement of HIV-1 infectivity. J Biol Chem 280(6):5032–5044. https://doi.org/10.1074/jbc.M401202200
12. Sanfridson A, Hester S, Doyle C (1997) Nef proteins encoded by human and simian immunodeficiency viruses induce the accumulation of endosomes and lysosomes in human T cells. Proc Natl Acad Sci U S A 94(3):873–878
13. Stumptner-Cuvelette P, Jouve M, Helft J, Dugast M, Glouzman AS, Jooss K, Raposo G, Benaroch P (2003) Human immunodeficiency virus-1 Nef expression induces intracellular accumulation of multivesicular bodies and major histocompatibility complex class II complexes: potential role of phosphatidylinositol 3-kinase. Mol Biol Cell 14(12):4857–4870. https://doi.org/10.1091/mbc.E03-04-0211
14. Costa LJ, Chen N, Lopes A, Aguiar RS, Tanuri A, Plemenitas A, Peterlin BM (2006) Interactions between Nef and AIP1 proliferate multivesicular bodies and facilitate egress of HIV-1. Retrovirology 3:33. https://doi.org/10.1186/1742-4690-3-33
15. Fevrier B, Raposo G (2004) Exosomes: endosomal-derived vesicles shipping extracellular messages. Curr Opin Cell Biol 16(4):415–421. https://doi.org/10.1016/j.ceb.2004.06.003
16. Lenassi M, Cagney G, Liao M, Vaupotic T, Bartholomeeusen K, Cheng Y, Krogan NJ, Plemenitas A et al (2010) HIV Nef is secreted in exosomes and triggers apoptosis in bystander CD4+ T cells. Traffic 11(1):110–122. https://doi.org/10.1111/j.1600-0854.2009.01006.x
17. Muratori C, Cavallin LE, Kratzel K, Tinari A, De Milito A, Fais S, D'Aloja P, Federico M et al (2009) Massive secretion by T cells is caused by HIV Nef in infected cells and by Nef transfer to bystander cells. Cell Host Microbe 6(3):218–230. https://doi.org/10.1016/j.chom.2009.06.009
18. Lee JH, Schierer S, Blume K, Dindorf J, Wittki S, Xiang W, Ostalecki C, Koliha N et al (2016) HIV-Nef and ADAM17-containing plasma extracellular vesicles induce and correlate with immune pathogenesis in chronic HIV infection. EBioMedicine 6:103–113. https://doi.org/10.1016/j.ebiom.2016.03.004
19. Lee JH, Wittki S, Brau T, Dreyer FS, Kratzel K, Dindorf J, Johnston IC, Gross S et al (2013) HIV Nef, paxillin, and Pak1/2 regulate activation and secretion of TACE/ADAM10 proteases. Mol Cell 49(4):668–679. https://doi.org/10.1016/j.molcel.2012.12.004
20. Puzar Dominkus P, Ferdin J, Plemenitas A, Peterlin BM, Lenassi M (2017) Nef is secreted in exosomes from Nef.GFP-expressing and HIV-1-infected human astrocytes. J Neurovirol. doi:https://doi.org/10.1007/s13365-017-0552-x
21. Raymond AD, Diaz P, Chevelon S, Agudelo M, Yndart-Arias A, Ding H, Kaushik A, Jayant RD et al (2016) Microglia-derived HIV Nef+ exosome impairment of the blood-brain barrier is treatable by nanomedicine-based delivery of Nef peptides. J Neurovirol 22(2):129–139. https://doi.org/10.1007/s13365-015-0397-0
22. Arenaccio C, Chiozzini C, Columba-Cabezas S, Manfredi F, Affabris E, Baur A, Federico M (2014) Exosomes from human immunodeficiency virus type 1 (HIV-1)-infected cells license quiescent CD4+ T lymphocytes to replicate HIV-1 through a Nef- and ADAM17-dependent mechanism. J Virol 88(19):11529–11539. https://doi.org/10.1128/JVI.01712-14
23. van Marle G, Henry S, Todoruk T, Sullivan A, Silva C, Rourke SB, Holden J, McArthur JC et al (2004) Human immunodeficiency virus type 1 Nef protein mediates neural cell death: a neurotoxic role for IP-10. Virology 329(2):302–318. https://doi.org/10.1016/j.virol.2004.08.024
24. Khan MB, Lang MJ, Huang MB, Raymond A, Bond VC, Shiramizu B, Powell MD (2016) Nef exosomes isolated from the plasma of individuals with HIV-associated dementia (HAD) can induce Abeta(1-42) secretion in SH-SY5Y neural cells. J Neurovirol 22(2):179–190. https://doi.org/10.1007/s13365-015-0383-6
25. Sami Saribas A, Cicalese S, Ahooyi TM, Khalili K, Amini S, Sariyer IK (2017) HIV-1 Nef is released in extracellular vesicles derived from astrocytes: evidence for Nef-mediated neurotoxicity. Cell Death Dis 8(1):e2542. https://doi.org/10.1038/cddis.2016.467
26. Garcia-Mesa Y, Jay TR, Checkley MA, Luttge B, Dobrowolski C, Valadkhan S, Landreth GE, Karn J et al (2017) Immortalization of primary microglia: a new platform to study HIV regulation in the central nervous system. J Neurovirol 23(1):47–66. https://doi.org/10.1007/s13365-016-0499-3
27. Nomaguchi M, Doi N, Matsumoto Y, Sakai Y, Fujiwara S, Adachi A (2012) Species tropism of HIV-1 modulated by viral accessory proteins. Front Microbiol 3:267. https://doi.org/10.3389/fmicb.2012.00267

28. Karris MA, Smith DM (2011) Tissue-specific HIV-1 infection: why it matters. Future Virol 6(7):869–882. https://doi.org/10.2217/fvl.11.48
29. Rigal A, Doyle SM, Robert S (2015) Live cell imaging of FM4-64, a tool for tracing the endocytic pathways in Arabidopsis root cells. Methods Mol Biol 1242:93–103. https://doi.org/10.1007/978-1-4939-1902-4_9
30. Kreft M, Milisav I, Potokar M, Zorec R (2004) Automated high through-put colocalization analysis of multichannel confocal images. Comput Methods Prog Biomed 74(1):63–67. https://doi.org/10.1016/S0169-2607(03)00071-3
31. Potokar M, Kreft M, Pangrsic T, Zorec R (2005) Vesicle mobility studied in cultured astrocytes. Biochem Biophys Res Commun 329(2):678–683. https://doi.org/10.1016/j.bbrc.2005.02.030
32. Raymond AD, Campbell-Sims TC, Khan M, Lang M, Huang MB, Bond VC, Powell MD (2011) HIV type 1 Nef is released from infected cells in CD45(+) microvesicles and is present in the plasma of HIV-infected individuals. AIDS Res Hum Retrovir 27(2):167–178. https://doi.org/10.1089/aid.2009.0170
33. Ali SA, Huang MB, Campbell PE, Roth WW, Campbell T, Khan M, Newman G, Villinger F et al (2010) Genetic characterization of HIV type 1 Nef-induced vesicle secretion. AIDS Res Hum Retrovir 26(2):173–192. https://doi.org/10.1089/aid.2009.0068
34. Lim JP, Gleeson PA (2011) Macropinocytosis: an endocytic pathway for internalising large gulps. Immunol Cell Biol 89(8):836–843. https://doi.org/10.1038/icb.2011.20
35. Vardjan N, Gabrijel M, Potokar M, Svajger U, Kreft M, Jeras M, de Pablo Y, Faiz M et al (2012) IFN-γ-induced increase in the mobility of MHC class II compartments in astrocytes depends on intermediate filaments. J Neuroinflammation 9:144. https://doi.org/10.1186/1742-2094-9-144
36. Pereira EA, daSilva LL (2016) HIV-1 Nef: taking control of protein trafficking. Traffic 17(9):976–996. https://doi.org/10.1111/tra.12412
37. Potokar M, Stenovec M, Gabrijel M, Li L, Kreft M, Grilc S, Pekny M, Zorec R (2010) Intermediate filaments attenuate stimulation-dependent mobility of endosomes/lysosomes in astrocytes. Glia 58(10):1208–1219. https://doi.org/10.1002/glia.21000
38. Stenovec M, Milošević M, Petrušić V, Potokar M, Stević Z, Prebil M, Kreft M, Trkov S et al (2011) Amyotrophic lateral sclerosis immunoglobulins G enhance the mobility of Lysotracker-labelled vesicles in cultured rat astrocytes. Acta Physiol (Oxf) 203(4):457–471. https://doi.org/10.1111/j.1748-1716.2011.02337.x
39. Stenovec M, Trkov S, Kreft M, Zorec R (2014) Alterations of calcium homoeostasis in cultured rat astrocytes evoked by bioactive sphingolipids. Acta Physiol (Oxf) 212(1):49–61. https://doi.org/10.1111/apha.12314
40. Stenovec M, Trkov S, Lasic E, Terzieva S, Kreft M, Rodriguez Arellano JJ, Parpura V, Verkhratsky A et al (2016) Expression of familial Alzheimer disease presenilin 1 gene attenuates vesicle traffic and reduces peptide secretion in cultured astrocytes devoid of pathologic tissue environment. Glia 64(2):317–329. https://doi.org/10.1002/glia.22931
41. Trkov S, Stenovec M, Kreft M, Potokar M, Parpura V, Davletov B, Zorec R (2012) Fingolimod—a sphingosine-like molecule inhibits vesicle mobility and secretion in astrocytes. Glia 60(9):1406–1416. https://doi.org/10.1002/glia.22361
42. Gerlach H, Laumann V, Martens S, Becker CF, Goody RS, Geyer M (2010) HIV-1 Nef membrane association depends on charge, curvature, composition and sequence. Nat Chem Biol 6(1):46–53. https://doi.org/10.1038/nchembio.268
43. Keppler OT, Allespach I, Schuller L, Fenard D, Greene WC, Fackler OT (2005) Rodent cells support key functions of the human immunodeficiency virus type 1 pathogenicity factor Nef. J Virol 79 (3):1655–1665. doi:https://doi.org/10.1128/JVI.79.3.1655-1665.2005
44. Majumdar A, Cruz D, Asamoah N, Buxbaum A, Sohar I, Lobel P, Maxfield FR (2007) Activation of microglia acidifies lysosomes and leads to degradation of Alzheimer amyloid fibrils. Mol Biol Cell 18(4):1490–1496. https://doi.org/10.1091/mbc.E06-10-0975
45. Deneka M, Pelchen-Matthews A, Byland R, Ruiz-Mateos E, Marsh M (2007) In macrophages, HIV-1 assembles into an intracellular plasma membrane domain containing the tetraspanins CD81, CD9, and CD53. J Cell Biol 177(2):329–341. https://doi.org/10.1083/jcb.200609050
46. Tan J, Sattentau QJ (2013) The HIV-1-containing macrophage compartment: a perfect cellular niche? Trends Microbiol 21(8):405–412. https://doi.org/10.1016/j.tim.2013.05.001
47. Pelchen-Matthews A, Giese S, Mlcochova P, Turner J, Marsh M (2012) beta2 integrin adhesion complexes maintain the integrity of HIV-1 assembly compartments in primary macrophages. Traffic 13(2):273–291. https://doi.org/10.1111/j.1600-0854.2011.01306.x
48. Jouve M, Sol-Foulon N, Watson S, Schwartz O, Benaroch P (2007) HIV-1 buds and accumulates in "nonacidic" endosomes of macrophages. Cell Host Microbe 2(2):85–95. https://doi.org/10.1016/j.chom.2007.06.011
49. Chu H, Wang JJ, Qi M, Yoon JJ, Wen X, Chen X, Ding L, Spearman P (2012) The intracellular virus-containing compartments in primary human macrophages are largely inaccessible to antibodies and small molecules. PLoS One 7(5):e35297. https://doi.org/10.1371/journal.pone.0035297
50. Mlcochova P, Pelchen-Matthews A, Marsh M (2013) Organization and regulation of intracellular plasma membrane-connected HIV-1 assembly compartments in macrophages. BMC Biol 11:89. https://doi.org/10.1186/1741-7007-11-89
51. Kyei GB, Dinkins C, Davis AS, Roberts E, Singh SB, Dong C, Wu L, Kominami E et al (2009) Autophagy pathway intersects with HIV-1 biosynthesis and regulates viral yields in macrophages. J Cell Biol 186(2):255–268. https://doi.org/10.1083/jcb.200903070
52. Arold S, Hoh F, Domergue S, Birck C, Delsuc MA, Jullien M, Dumas C (2000) Characterization and molecular basis of the oligomeric structure of HIV-1 nef protein. Protein Sci 9(6):1137–1148. https://doi.org/10.1110/ps.9.6.1137
53. Soldati T, Schliwa M (2006) Powering membrane traffic in endocytosis and recycling. Nat Rev Mol Cell Biol 7(12):897–908. https://doi.org/10.1038/nrm2060
54. Potokar M, Kreft M, Li L, Daniel Andersson J, Pangrsic T, Chowdhury HH, Pekny M, Zorec R (2007) Cytoskeleton and vesicle mobility in astrocytes. Traffic 8(1):12–20. https://doi.org/10.1111/j.1600-0854.2006.00509.x
55. Ichikawa T, Yamada M, Homma D, Cherry RJ, Morrison IE, Kawato S (2000) Digital fluorescence imaging of trafficking of endosomes containing low-density lipoprotein in brain astroglial cells. Biochem Biophys Res Commun 269(1):25–30. https://doi.org/10.1006/bbrc.2000.2261
56. Thompson GL, Roth CC, Dalzell DR, Kuipers M, Ibey BL (2014) Calcium influx affects intracellular transport and membrane repair following nanosecond pulsed electric field exposure. J Biomed Opt 19(5):055005. https://doi.org/10.1117/1.JBO.19.5.055005
57. Weisenberg RC (1972) Microtubule formation in vitro in solutions containing low calcium concentrations. Science 177(4054):1104–1105
58. O'Brien ET, Salmon ED, Erickson HP (1997) How calcium causes microtubule depolymerization. Cell Motil Cytoskeleton 36(2):125–135. https://doi.org/10.1002/(SICI)1097-0169(1997)36:2<125::AID-CM3>3.0.CO;2-8

59. Deery WJ, Means AR, Brinkley BR (1984) Calmodulin-microtubule association in cultured mammalian cells. J Cell Biol 98(3):904–910
60. Lieuvin A, Labbe JC, Doree M, Job D (1994) Intrinsic microtubule stability in interphase cells. J Cell Biol 124(6):985–996
61. El-Hage N, Rodriguez M, Dever SM, Masvekar RR, Gewirtz DA, Shacka JJ (2015) HIV-1 and morphine regulation of autophagy in microglia: limited interactions in the context of HIV-1 infection and opioid abuse. J Virol 89(2):1024–1035. https://doi.org/10.1128/JVI.02022-14
62. Klionsky DJ, Emr SD (2000) Autophagy as a regulated pathway of cellular degradation. Science 290(5497):1717–1721
63. Saribas AS, Khalili K, Sariyer IK (2015) Dysregulation of autophagy by HIV-1 Nef in human astrocytes. Cell Cycle 14(18):2899–2904. https://doi.org/10.1080/15384101.2015.1069927
64. Kimura S, Noda T, Yoshimori T (2007) Dissection of the autophagosome maturation process by a novel reporter protein, tandem fluorescent-tagged LC3. Autophagy 3(5):452–460
65. Campbell TD, Khan M, Huang MB, Bond VC, Powell MD (2008) HIV-1 Nef protein is secreted into vesicles that can fuse with target cells and virions. Ethn Dis 18(2 Suppl 2): S2-14–S2-19
66. Momen-Heravi F, Balaj L, Alian S, Mantel PY, Halleck AE, Trachtenberg AJ, Soria CE, Oquin S et al (2013) Current methods for the isolation of extracellular vesicles. Biol Chem 394(10):1253–1262. https://doi.org/10.1515/hsz-2013-0141
67. Krzan M, Stenovec M, Kreft M, Pangrsic T, Grilc S, Haydon PG, Zorec R (2003) Calcium-dependent exocytosis of atrial natriuretic peptide from astrocytes. J Neurosci 23(5):1580–1583
68. Dou Y, Wu HJ, Li HQ, Qin S, Wang YE, Li J, Lou HF, Chen Z et al (2012) Microglial migration mediated by ATP-induced ATP release from lysosomes. Cell Res 22(6):1022–1033. https://doi.org/10.1038/cr.2012.10
69. Epstein LG, Gelbard HA (1999) HIV-1-induced neuronal injury in the developing brain. J Leukoc Biol 65(4):453–457